Supplementary Information for

Inhibition of histone H3K27 demethylases inactivates brachyury (TBXT) and promotes chordoma cell death

Lucia Cottone, Adam P Cribbs, Garima Khandelwal, Graham Wells, Lorena Ligammari, Martin Philpott, Anthony Tumber, Patrick Lombard, Edward S Hookway, Tamas Szommer, Catrine Johansson, Paul E Brennan, Nischalan Pillay, Richard G Jenner, Udo Oppermann, Adrienne M Flanagan

This PDF file includes:

Figures S1 to S7
Tables S1 to S5
Captions for Datasets S1 to S3
Supplementary text
References for Supplementary Information

Other supplementary materials for this manuscript include the following:

Datasets S1 to S3

Supplementary Figures

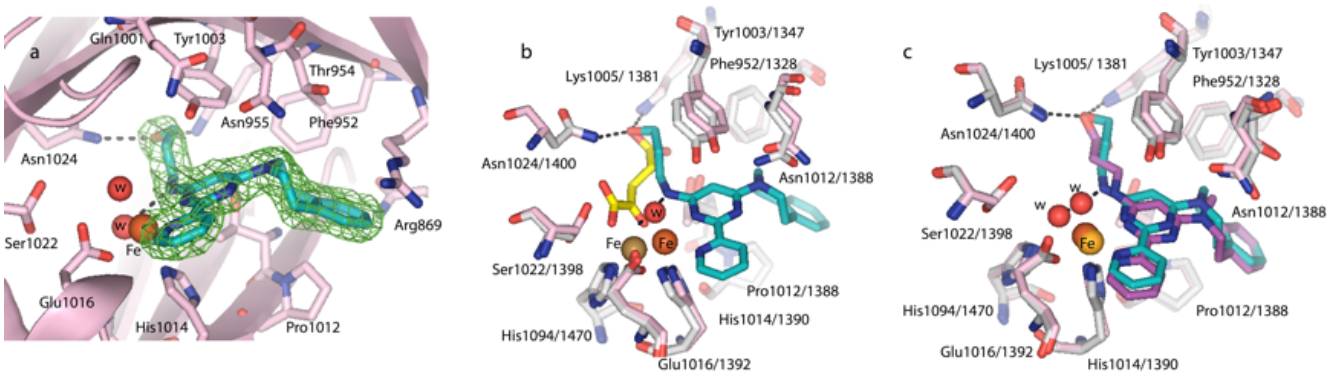

Figure S1. Ligand structure of human UTY (KDM6C) in complex with KDOBA67. Crystal structure of UTY in complex with the inhibitor KDOBA67a shows identical ligand binding as KDM6B/GSK-J1. (**A**) Representation of the ligand binding pocket in UTY (pdb 5A1L, rendered in pink) in complex with KDOBA67a (cyan). Amino acid side-chains lining the active site are depicted as sticks. The position of the catalytic metal ion and water molecules are shown as orange/brown spheres. The 2FoFc electron density map is contoured at 1.0 sigma. (**B**) KDOBA67 occupies part of the cofactor site in KDM6 enzymes, demonstrated through an overlay of UTY(pdb 5A1L, pink) with KDM6B (grey) in complex with the 2'oxoglutarate cofactor (yellow) (PDB 2XUE). (**C**) KDOBA67 shows equivalent occupation and residue contacts in the active site of KDM6 enzymes, demonstrated through an overlay of UTY/KDOBA67 and KDM6B/GSK-J1 (magenta) (PDB 4ASK) complexes.

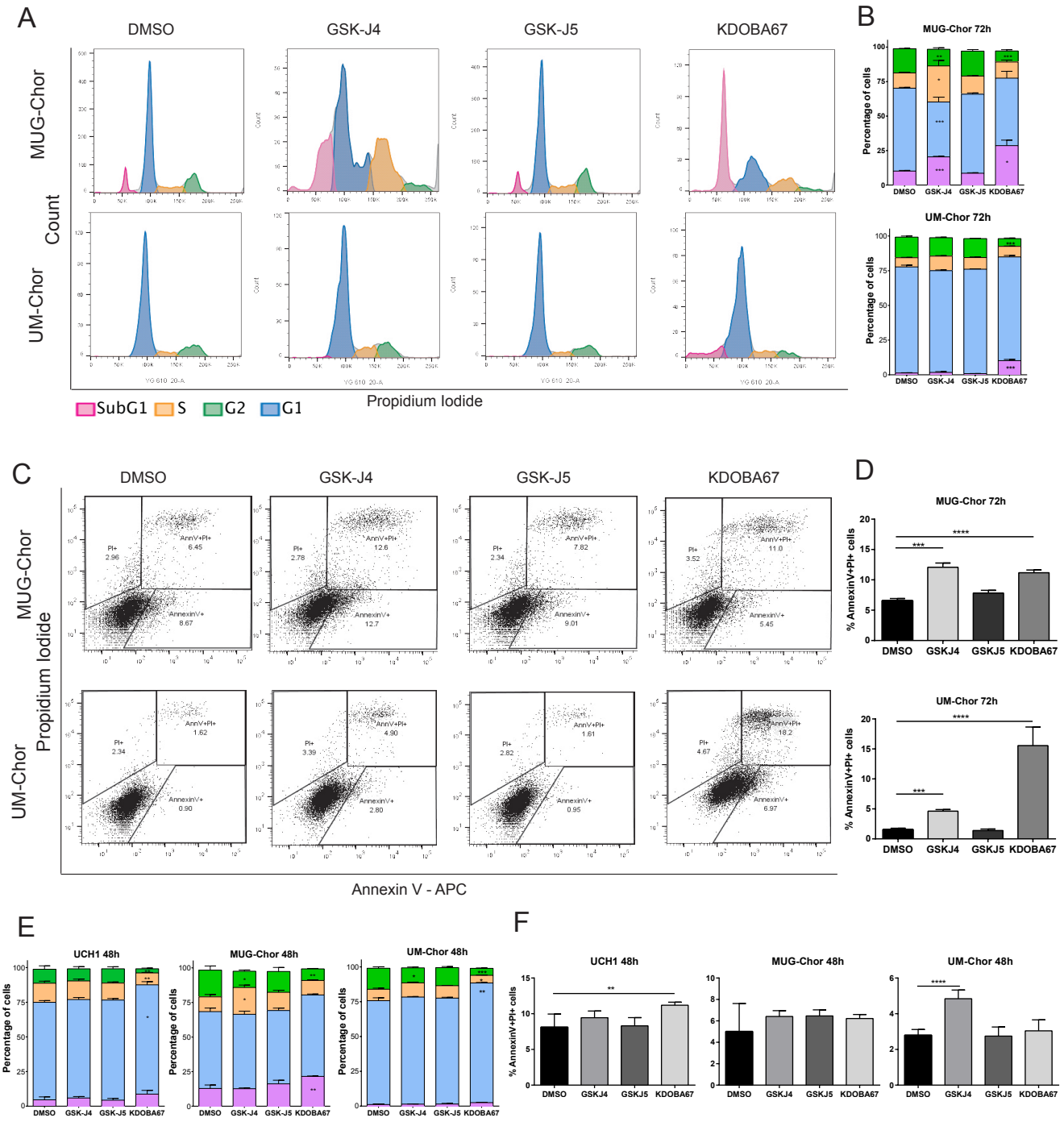

Figure S2. H3K27 lysine demethylase inhibitors induce cell cycle arrest and apoptosis in chordoma cell lines. (A-D) Cell cycle changes (A-B) and cell death analysis (C-D) in UM-Chor and MUG-Chor following 72 hours of exposure to the compounds. By 72 hours, there is evidence of apoptosis as determined by an increase in sub-G1 and in AnnexinV-PI-positive population in response to GSK-J4 and KDOBA67. **(E-F)** Cell cycle changes (E) and cell death analysis (F) in UCH1, UM-Chor and MUG-Chor following 48 hours of treatment with the compounds at which time there is a significant increase in the G1 population and reduction in the S population in UCH1 and UM-Chor only, and a significant increase in sub-G1 population in MUG-Chor. There is a slight increase in the AnnexinV-PI-positive population in response to GSK-J4 and KDOBA67. Representative histogram/dot plots and quantification of 3 independent experiments, with 3 replicates per condition per experiment. *p ≤0.05, **p ≤0.01, ***p ≤0.001, ****p ≤0.0001.

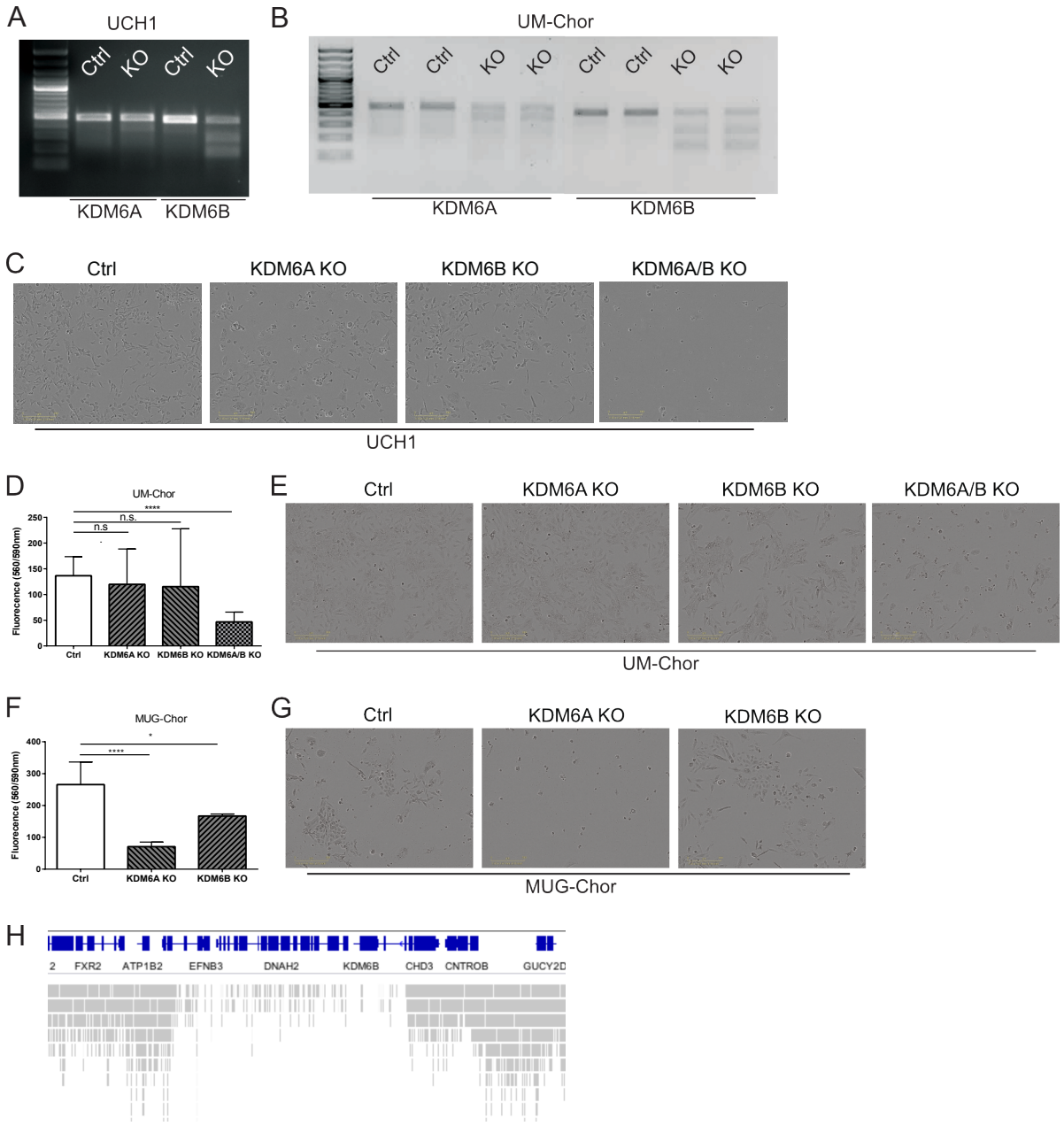

Figure S3. CRISPR/Cas9 mediated *KDM6A* and *KDM6B* knockout. (A-B) Cleavage assay for UCH1 and UM-Chor for cells transduced with empy-Lenti-Cas9-vector (Control, ctrl), guideRNA-directed at *KDM6A* or *KDM6B*, show efficient gene editing at the predicted site. **(C)** Bright field images of UCH1 with CRISPR editing of *KDM6A/B* and both. **(D-E)** CRISPR/Cas9 knock-out of *KDM6A* and *KMD6B* induces cell growth arrest in UM-Chor chordoma cell line. Cell viability and representative images of chordoma cells transduced with empy-Lenti-Cas9-vector, guideRNA-directed towards *KDM6A*, *KDM6B* or co-transduced with both. (**F-H**) In MUG-Chor cell line knock-out of *KDM6A* is sufficient to reduce cell viability, because MUG-Chor contains a biallelic deletion of *KDM6B* as visualised by genome sequencing generated from the ChIP input in (H). Quantification of 2 independent experiments, with 2 biological replicates per condition. *p ≤0.05, **p ≤0.01, ***p ≤0.001, ****p ≤0.0001.

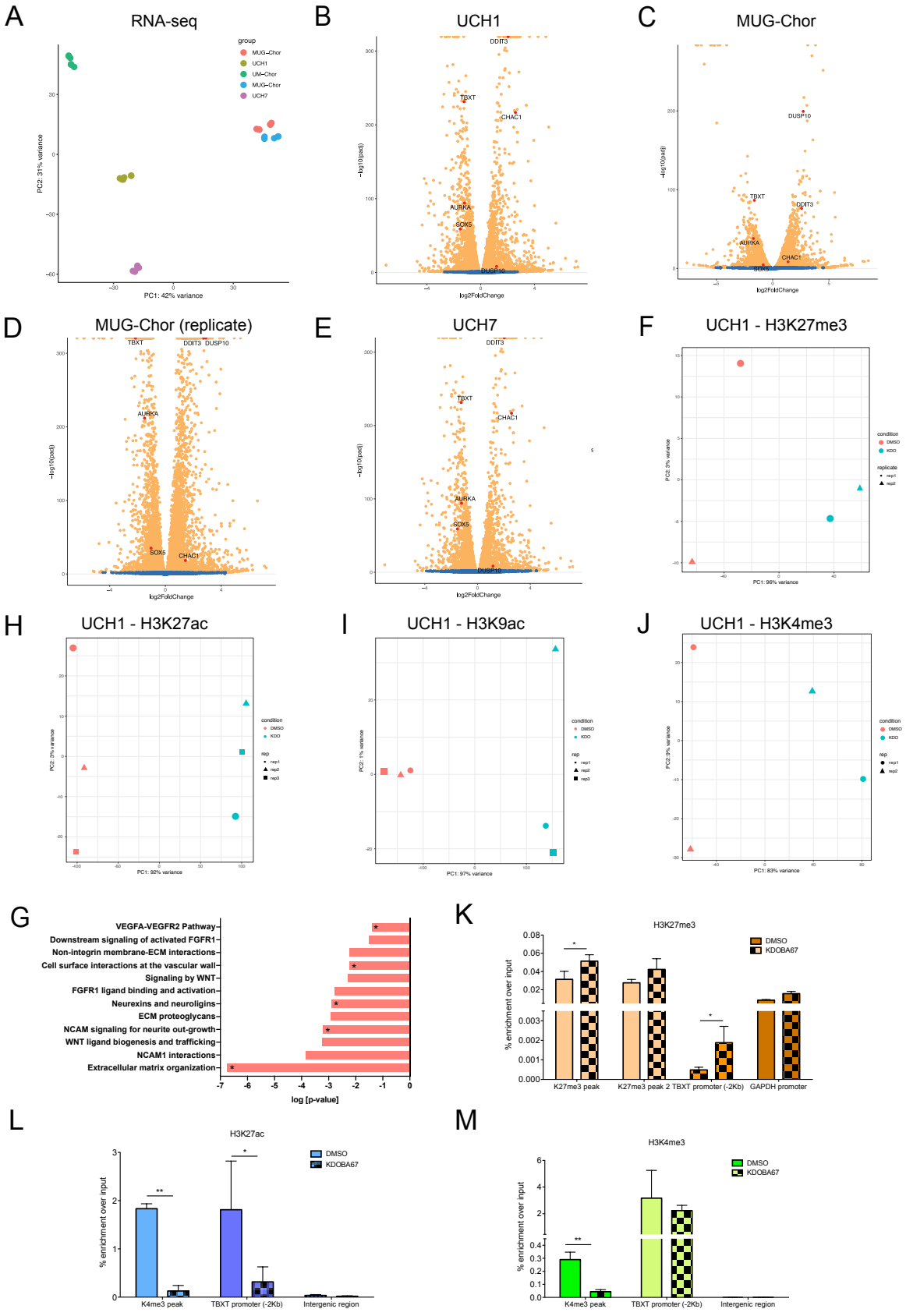
A
RNA-seq
group
MUG–Chor
UCH1
UM–Chor
MUG–Chor
UCH7
PC2: 31% variance
PC1: 42% variance
B
UCH1
DDIT3
TBXT
CHAC1
AURKA
SOX5
DUSP10
−log10(padj)
log2FoldChange
C
MUG-Chor
DUSP10
TBXT
DDIT3
AURKA
CHAC1
SOX5
−log10(padj)
log2FoldChange
D
MUG-Chor (replicate)
TBXT
DDIT3
DUSP10
AURKA
SOX5
CHAC1
−log10(padj)
log2FoldChange
E
UCH7
DDIT3
TBXT
CHAC1
AURKA
SOX5
DUSP10
−log10(padj)
log2FoldChange
F
UCH1 - H3K27me3
condition
DMSO
KDO
replicate
rep1
rep2
PC2: 3% variance
PC1: 96% variance
H
UCH1 - H3K27ac
condition
DMSO
KDO
rep
rep1
rep2
rep3
PC2: 3% variance
PC1: 92% variance
I
UCH1 - H3K9ac
condition
DMSO
KDO
rep
rep1
rep2
rep3
PC2: 1% variance
PC1: 97% variance
J
UCH1 - H3K4me3
condition
DMSO
KDO
rep
rep1
rep2
PC2: 9% variance
PC1: 83% variance
G
VEGFA-VEGFR2 Pathway
Downstream signaling of activated FGFR1
Non-integrin membrane-ECM interactions
Cell surface interactions at the vascular wall
Signaling by WNT
FGFR1 ligand binding and activation
Neurexins and neuroligins
ECM proteoglycans
NCAM signaling for neurite out-growth
WNT ligand biogenesis and trafficking
NCAM1 interactions
Extracellular matrix organization
log [p-value]
K
H3K27me3
DMSO
KDOBA67
% enrichment over input
K27me3 peak
K27me3 peak 2
TBXT promoter (-2Kb)
GAPDH promoter
L
H3K27ac
DMSO
KDOBA67
% enrichment over input
K4me3 peak
TBXT promoter (-2Kb)
Intergenic region
M
H3K4me3
DMSO
KDOBA67
% enrichment over input
K4me3 peak
TBXT promoter (-2Kb)
Intergenic region

Figure S4. **Transcriptomic and ChIP analysis of chordoma cell lines in response to KDOBA67.** (**A**) PCA plot of all RNA sequencing data for UCH1, UCH7, MUG-Chor, UM-Chor, 3 biological replicates per cell lines per treatment. Two independent datasets were generated for MUG-Chor, and the very close clustering shows high reproducibility of the data. (**B-E**) Volcano plot summarising differential gene expression in chordoma cells following treatment with KDOBA67 for 48 hours, by RNA-seq. (**F** and **H-J**) PCA plot of all ChIP-Rx data of UCH1. For H3K27me3 and H3K4me3 only 2 out of 3 replicates per treatment were of good quality and have been used for the analysis. (**G**) Reactome analysis for H3K27me3 differentially bound peaks in UCH1 in response to KDOBA67. Asterisks (*) mark pathways also identified in the Reactome analysis of RNA-seq data for UCH1. See also **Dataset S3**. (**K-M**) ChIP-qPCR results of H3K27me3, H3K27ac and H3K4me3 for UM-Chor cells following treatment with KDOBA67 for 48 hours. TBXT promoter region analysed is -2Kb from the TSS. K27me3 peak1, K27me3 peak2 and K4me3 peak are positive peaks identified in UCH1 by ChIP-Rx. Results from 4 biological replicates per condition. *p ≤0.05, **p ≤0.01, ***p ≤0.001, ****p ≤0.0001.

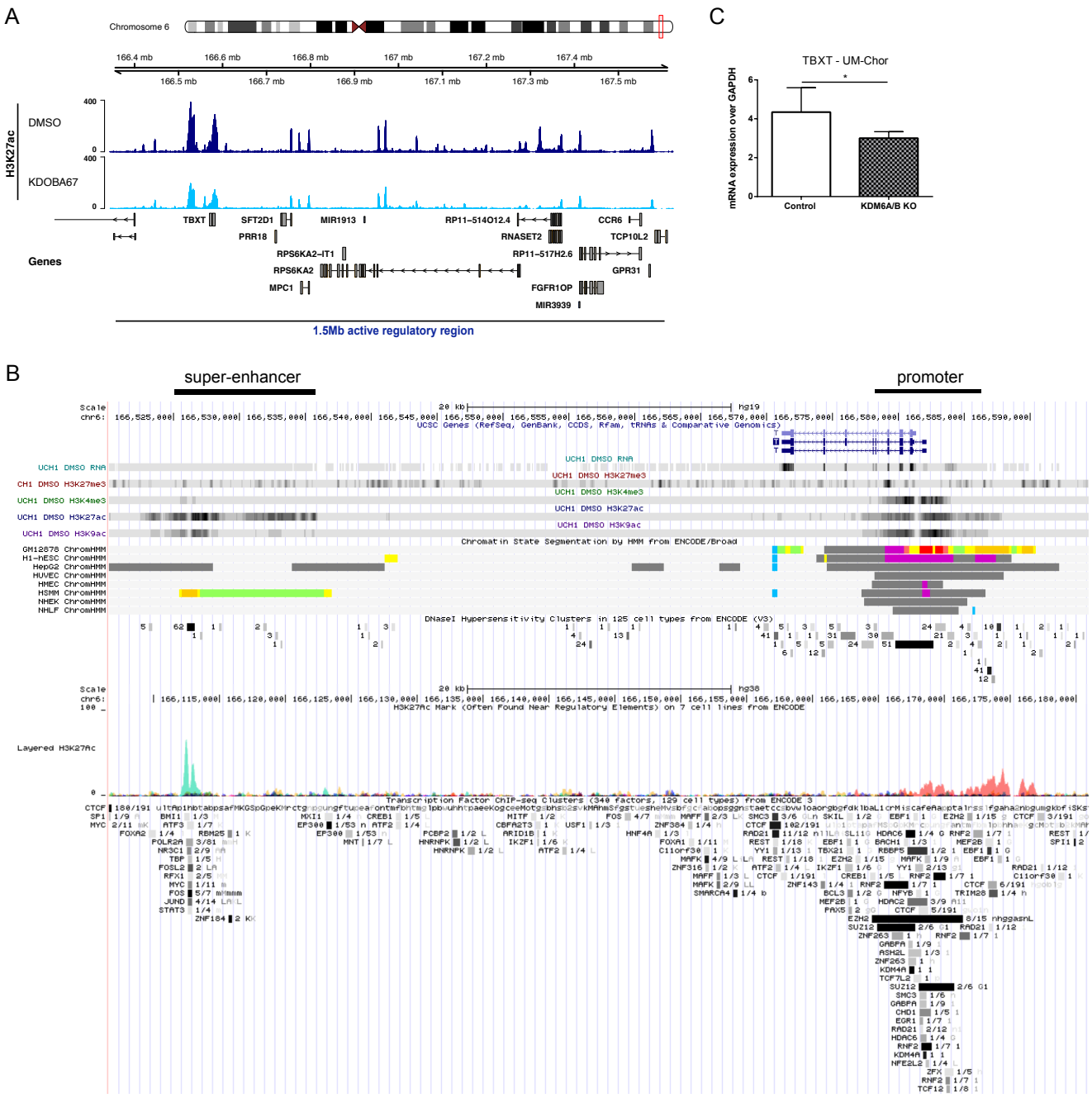

Figure S5. Specific inhibition of H3K27 lysine demethylase leads to changes in the *TBXT* regulatory region. **(A)** H3K27ac tracks for UCH1 showing a reduction in the previously described 1.5Mb active regulatory region around *TBXT*. Tracks show the average of 3 biological replicates. **(B)** Visualization of the regulatory region around *TBXT* including at the promoter and super-enhancer in the UCH1 cell line (our data, top 5 tracks) and in publicly available ENCODE datasets. Chromatin State Segmentation by HMM from ENCODE/Broad (1) shows that an active promoter (red/purple) is present at the promoter region and that a strong enhancer (yellow) is detected in the super-enhancer region. These two regions are also characterised by several DNaseI hypersensitivity sites (2,3), H3K27ac enrichment and binding of several transcription factors (including CTCF and EZH2) in 129 cell lines reported in the ENCODE project (4). **(C)** Expression of *TBXT* is reduced in UM-Chor upon double knock-out (KO) of *KDM6A/B*, as assessed by qPCR. Quantification of 2 independent experiments, with 2 biological replicates per condition. *p ≤0.05, **p ≤0.01, ***p ≤0.001, ****p ≤0.0001.

Figure S6. Methylation profiles of *TBXT* promoter in a range of solid tumours. Data from the Cancer Tumor Genome Atlas (TCGA) showed that the promoter of *TBXT* is unmethylated is a variety of malignancies, known not to express TBXT. Low levels of methylation are prominent in cervical squamous cell carcinomas, diffuse B cell lymphomas and adenocarcinomas of the gastrointestinal tract, tumours which are rarely reported to express TBXT protein.

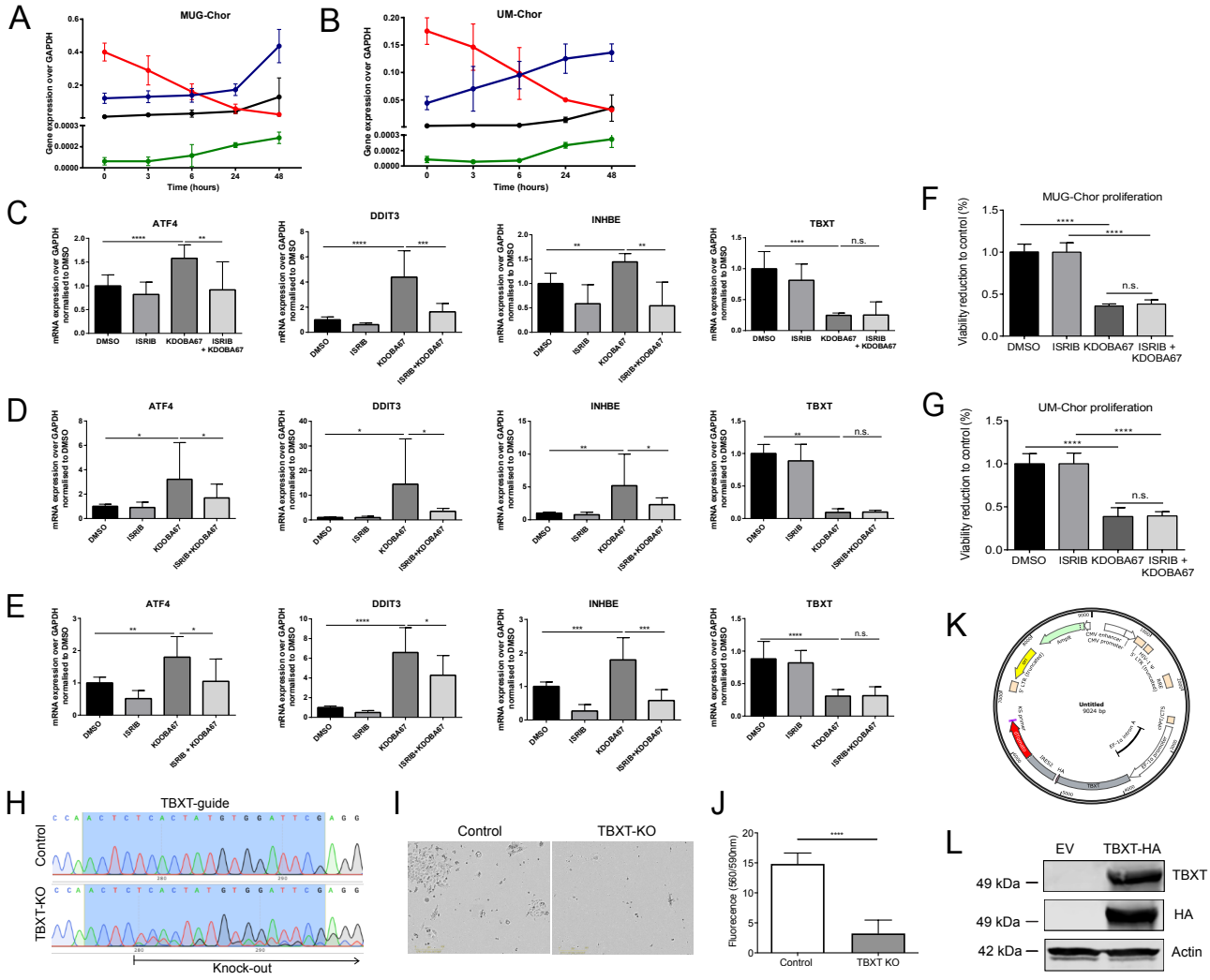

Figure S7. The ATF4-response is activated in patient-derived primary chordoma cell cultures and two additional chordoma cell lines but does not contribute to *TBXT* suppression in response to KDOBA67. **(A-B)** Expression of *TBXT*, *ATF4* and ATF4-target genes *DDIT3*, *INHBE* over a time course in response to KDOBA67 in UCH1, MUG-Chor and UM-Chor as assessed by qPCR. Results from 2 independent experiments, with 3 replicates per condition per cell line. (**C-E**) Co-treatment of KDOBA67 and ISRIB for 48 hours suppresses the induction of *ATF4* and ATF4-target genes (*DDIT3*, *INHBE*) but does not prevent the downregulation of *TBXT* induced by KDOBA67, as assessed by qPCR in UCH1 (C) MUG-Chor (D) and UM-Chor (E). Results from 3 independent experiments, with 3 biological replicates per condition. (**F-G**) Proliferation in response to KDOBA67 in the presence of ISRIB as assessed by Presto Blue assay in MUG-Chor (F) and UM-Chor (G). Results from 3 independent experiments, with 3 biological replicates per condition. (**H**) Sanger sequencing of MUG-Chor cells transduced with empy-Lenti-Cas9-vector (Control) and Lenti-Cas9-vector with guideRNA-directed at *TBXT* (TBXT-KO) (guide highlighted in blue) shows efficient gene editing at the predicted knock out site. (**I**) Bright field images of MUG-Chor following CRISPR /Cas9 editing of *TBXT* and Control. (**J**) Knock-out of *TBXT* induces cell growth arrest in MUG-Chor chordoma cell line, assessed by Presto Blue proliferation. 6 replicates. (**K-L**) Map of the expression vector containing TBXT-HA-dTomato (K) and expression of *TBXT* together with HA tag at the protein level following expression of the vector in HEK-293T cells by western blot, where beta actin is used as an endogenous control (L). *p ≤0.05, **p ≤0.01, ***p ≤0.001, ****p ≤0.0001.

Supplementary Tables

Table S1. STR (Short Tandem Repeat) analysis results for UCH1, MUG-Chor, UM-Chor and UCH7 used in the study (most recent results obtained in March 2018 for MUG-Chor, UM-Chor, UCH7 and in December 2019 for UCH1).

		UCL profiles		Database profiles	
Cell line	Marker	Allele 1	Allele 2	Allele 1	Allele 2
UCH1	AMEL	X	Y	X	Y
	CSF1PO	10	11	10	11
	D13S317	11	13	11	13
	D16S539	12	13	12	13
	D18S51	15	15	15	15
	D21S11	28	29	28	29
	D3S1358	15	15	15	15
	D5S818	11	12	11	12
	D7S820	9	12	9	12
	D8S1179	10	15	10	15
	FGA	20	21	20	21
	Penta D	11	11	11	11
	Penta E	7	10	7	10
	TH01	7	7	7	7
	TPOX	8	11	8	11
	vWA	17	17	17	17
	AMEL	X	X	X	X
MUG-Chor	CSF1PO	11	11	11	11
	D13S317	11	11	11	11
	D16S539	11	14	11	14
	D18S51	17	23	17	23
	D21S11	29	33.2	29	33.2
	D3S1358	14	17	14	17
	D5S818	11	12	11	12
	D7S820	8	11	8	11
	D8S1179	11	12	11	12
	FGA	21	26	21	26
	Penta D	13	13	13	13
	Penta E	5	12	5	12
	TH01	9.3	9.3	9.3	9.3
	TPOX	8	8	8	8
	vWA	15	15	15	15
UM-Chor	AMEL	X	Y	X	Y
	CSF1PO	11	12	11	12
	D13S317	12	12	12	12
	D16S539	12	12	12	12
	D18S51	14	14	14	14
	D21S11	27	31	27	31
	D3S1358	18	18	18	18
	D5S818	9	13	9	13
	D7S820	11	11	11	11
	D8S1179	12	13	12	13
	FGA	23	23	19	23
	Penta D	8	9	8	9
	Penta E	7	7	7	7
	TH01	7	9.3	7	9.3
	TPOX	8	9	8	9
	vWA	15	15	15	15
UCH-7	AMEL	17			
	CSF1PO	7			
	D13S317	30	33.2		
	D16S539	16			

	D18S51	12	15		
	D21S11	12	13		
	D3S1358	10			
	D5S818	10	11		
	D7S820	10	12		
	D8S1179	12			
	FGA	12	13		
	Penta D	X	Y		
	Penta E	16	17		
	TH01	14	16		
	TPOX	8	11		

Table S2. Table of IC50 values against selected KDM members as determined by Alphascreen (values in μM).

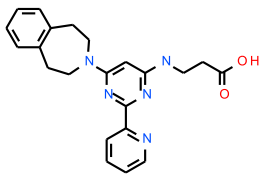

GSK-J1

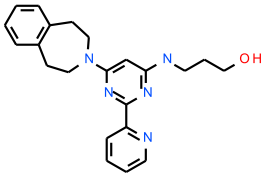

KDOBA67

	KDM3	KDM4	KDM5	KDM5	KDM5	KDM6
	JmjD1	JmjD2C	JARID1A	JARID1B	JARID1C	JmjD3
GSK-J1	>10	>10	2.5	0.4	1.3	0.16
GSK-J4	>100	>100	>100	>100	>100	>100
KDOBA67	>100	>100	24.0	28.2	62	0.24

Table S3: X-ray data collection and refinement statistics for human UTY (KDM6C) in complex with KDOBA67 (pdb 5A1L).

Data collection	
Space group	$P2_12_12_1$
Cell dimensions	
a, *b*, *c* (Å)	90.71, 110.5 ,119.46
α, β, γ (°)	90, 90, 90
Resolution (Å)	29.31 - 2 (2.0 - 2.11)
R_{merge}	0.019 (*0.89)*
Mean I / σ*I*	2.3
Completeness (%)	99.4 (99.4)
Redundancy	6.2 (5.8)
Refinement	
Resolution (Å)	2.0
No. reflections	76980
R_{work} / R_{free}	0.188/0.225
No. atoms	
Protein	7044
Ligand/ion	104
Water	680
B-factors	
Protein	36.70
Ligand/ion	51.00
Water	42.70
R.m.s deviations	
Bond lengths (Å)	0.019
Bond angles (°)	1.33

Table S4. List of antibodies used in this study

Protein	Kda	Brand	Cat. Number	Species	Clonality	Dilution
ChIP						
HA tag		Abcam	Ab9110	Rabbit		
H3 Total		Abcam	Ab 1791			
H3K27me3		Millipore	07-449	Rabbit		
IgG control (anti-mouse IgG (Z0259)		Dako	Z0259	Rabbit	Polyclonal	
H3K9me2		Millipore	17-648			
H3K4me3		Millipore	07-473	Rabbit	Polyclonal	
H3K4me3		Abcam	ab8580	Rabbit	Polyclonal	
H3K27ac		Abcam	Ab4729	Rabbit	Polyclonal	
H3K9ac		Abcam	Ab4441	Rabbit	Polyclonal	
KDM6A/UTX		Abcam	ab36938	Rabbit	Polyclonal	
KDM6B/Jmjd3		Abcam	ab38113	Rabbit	Polyclonal	
Western Blot						
B-actin	42	Sigma	A5441	Mouse	Monoclonal	1:5000
Brachyury (A-4)	49	Santa Cruz Biotechnology	Sc-374321	Mouse	Monoclonal	1:1000
HA-tag		Abcam	Ab9110	Rabbit	Polyclonal	
Immunofluorescence						
Brachyury (A-4)		Santa Cruz Biotechnology	Sc-374321	Mouse	Monoclonal	1:250
Anti-mouse-Alexa488		Thermo Fisher Scientific		Rabbit		1:500

Table S5. List of primers used in this study.

Gene	Application	Fw Primer	Rev primer
TBXT	qPCR	CCCGTCTCCTTCAGCAAAGTC	TGGATTCGAGGCTCATACTTATGC
GAPDH	qPCR	GCACCGTCAAGGCTGAGAAC	TGGTGAAGACGCCAGTGGA
ATF4	qPCR	ATGACCGAAATGAGCTTCCTG	GCTGGAGAACCCATGAGGT
DDIT3	qPCR	ATGAACGGCTCAAGCAGGAA	GCAGATTCACCATTCGGTCAA
INHBE	qPCR	CTCTGCCCTCTAGTGGCTTGA	CGCCTCGGTTGTCCAGTAA
MT1X	qPCR	ACGCTTTTCATCTGTCCCGC	GGGTCCATTTCGAGGCAAGG
KDM6A	qPCR	AGCGCAAAGGAGCCGTGGAAAA	GTCGTTCACCATTAGGACCTGC
KDM6B	qPCR	GACCCTCGAAATCCCATCACAG	GTGCGAACTTCCACGGTGTGTT
TBXT nascent RNA	qPCR	GCCTCCTCACCATCTCCAC	CCTCCTGCACTGAAACCCTT
ACTB nascent RNA	qPCR	AGCACAGAGCCTCGCCTTT	TCATCCATGGTGAGCTGGC
ATF4 nascent RNA	qPCR	CGTATTTGGACGTGGGGACG	ACAAAATGGACGCTCACGGA
DDIT3 nascent RNA	qPCR	CGTCCGAAGCAATAGGGGTT	AAGTTAGGGACCGTCCGAGA
INHBE nascent RNA	qPCR	CTTTCGGGCAGACTCCACTT	ATGGTACAGGTGGTGGGACC
TBXT promoter -1Kb	ChIP-PCR	GAGAAGGGAGAGAAGGAGCC	TTTCCCGCGGACATGGTAT
TBXT promoter -2Kb	ChIP-PCR	AAGCATGTTTTCGGTGGGAC	TAACAATGCGCTTCCTTGGG
TBXT exon 3	ChIP-PCR	AACGCCATGTACTCCTTCCT	CCGTTGAGCTTGTTGGTGAG
HOXA7 promoter -1Kb	ChIP-PCR	AGAGAGATTGCCACCGCAAA	TCACTGCTTCCTTTAGGGCG
TBXT Intergenic region +300Kb	ChIP-PCR	CACACCTGGATTGGCAATGG	CCTGCACCTTTCCTACCTGA
TBXT Super-enhancer	ChIP-PCR	GCAGGTCAGAAACACAGGTC	TGCACTTGACTTCCTTTGCC
GAPDH Promoter	ChIP-PCR	ATGTAGACCCCTTGAAGAGG	GGTTGAGCACAGGGTACTTT
K27me3 peak 1	ChIP-PCR	CATCGGGCTTCAGTAGTTGC	TCTCCACTGGCCCAAAAGAT
K27me3 peak 2	ChIP-PCR	CATCGGGCTTCAGTAGTTGC	TCTCCACTGGCCCAAAAGAT
K4me3 peak	ChIP-PCR	CTAGCCCAGGTGAAGGACAT	CCCAAATGCTTCAGGAGAGC
CRISPR guide KDM6A	CRISPR	CAGCATTATCTGCATACCAG (5)	
CRISPR guide KDM6B	CRISPR	GACAAAAGTACTGTTATCGG (6)	
CRISPR guide TBXT	CRISPR	CGAATCCACATAGTGAGAGT	

Captions for Supplementary Datasets

Dataset S1. List of compounds used in the compound drug screen including screening concentration, supplier, references and proliferation raw data (related to Fig. 1A). Attached as separate file (Excel).

Dataset S2. List of differentially expressed genes and differentially enriched pathways (Reactome) in all chordoma cell lines in response to treatment with KDOBA67 for 48 hours. Attached as separate file (Excel).

Dataset S3. List of differentially pathways (Reactome) overlapping with differentially enriched H3K27me3 peaks in UCH1 in response to treatment with KDOBA67 for 48 hours. Attached as separate file (Excel).

Supplementary Text

SI Materials and Methods

Chromatin Immunoprecipitation. Cells were fixed in 1% formaldehyde for 10 minutes prior to quenching with excess glycine. Cells were resuspended on ice in a cell lysis buffer (10 mM Tris-HCL, 10 mM Nacl, 0.5 % NP-40, all reagents were from Sigma-Aldrich) for 15 minutes, centrifuged, and resuspended in nuclear lysis buffer (50 mM Tris-HCl, 10 mM EDTA, 1 % SDS, all from Sigma-Aldrich) for 10 minutes. Samples were diluted with 2 volumes of dilution buffer (16.7 mM Tris-HCL, 167 mM NaCl, 1.2 mM EDTA, 0.01 % SDS, all from Sigma-Aldrich) and sonicated on a Bioruptor Pico (Diagenode, Belgium) for 10 cycles of 30 seconds on/30 seconds off. Sonication efficiency was checked by running a sample of de-crosslinked material on a 2 % agarose gel. Samples were incubated overnight rotating at 4ºC using antibody pre-incubated with protein A/G magnetic beads. Beads were washed sequentially with buffer 1 (50 mM Tris, 500 mM NaCl, 1 mM EDTA, 1 % Triton X-100, 0.1 % sodium deoxycholate, 0.1 % SDS, all from Sigma-Aldrich) three times, buffer 2 (20 mM Tris, 1 mM EDTA, 250 mM LiCl, 0.5% NP-40, 0.5% sodium deoxycholate, all from Sigma-Aldrich) three times and twice with TE buffer + 50 mM NaCl. DNA was eluted in buffer containing 50 mM Tris, 10 mM EDTA and 1% SDS before treatment with proteinase K and RNAse-A (both Thermo Fisher Scientific). DNA was eluted and de-crosslinked from beads prior to purification using home made Solid Phase Reversible Immobilization (SPRI) magnetic beads (prepared as previously described(7)). In order to perform ChIP for H3.3, cells lines (UCH1, UM-Chor, MUG-Chor and U2OS) were transduced with a lentiviral vector containing full length human *H3F3A* tagged with Hemagglutinin (HA). Transduced cells were FACS-sorted based on a fluorescent marker and processed for ChIP analysis.

Synthesis of compound: KDOBA67

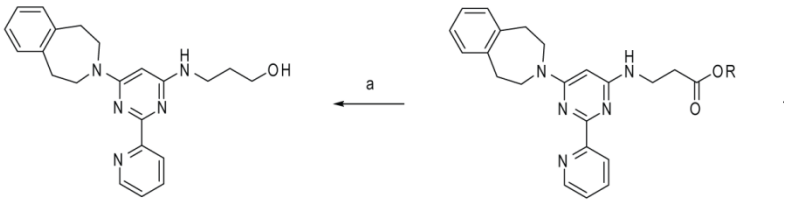

Reagents and conditions: (a) $LiAlH_4$, Et_2O, THF, 61%; THF, 34%.

3-{[2-(pyridin-2-yl)-6-(1,2,4,5-tetrahydro-3H-benzo[d]azepin-3-yl)pyrimidin-4-yl]amino}propan-1-ol (KDOBA67).

Method: GSK-J4 was synthesised as previously reported (8). To a mixture of $LiAlH_4$ (28 mg, 0.72 mmol) in 3 mL of Et_2O at 0 °C was added dropwise a solution of GSK-J4 (100 mg, 0.24 mmol) in 2 mL of Et_2O and 2 mL of THF. After 1 h at 0 °C the mixture was filtered and the filtrate was washed with CH_2Cl_2 (2x 20mL). The combined organic extracts were dried over Na_2SO_4, filtered, and evaporated *in vacuo*. The residue was purified by flash chromatography on silica gel (CH_2Cl_2/MeOH 30:1) to afford the title compound (59 mg, 61%).

MS (ESI): m/z calcd. for $(C_{22}H_{25}N_5O+H)^+$ 375.5, found 376.2.

^{1}H-NMR (300 MHz, $CDCl_3$) δ 8.74 (m, 1H), 8.43 (m, 1H), 7.83 – 7.72 (m, 1H), 7.32 (m, 1H), 7.16 – 7.09 (m, 4H), 5.54 (s, 1H), 5.17 (s, 1H), 3.96 – 3.84 (m, 4H), 3.71 – 3.58 (m, 4H), 3.03 – 2.92 (m, 4H), 1.82 – 1.66 (m, 2H).

IC_{50} Determination of GSK-J1 analogs. The potency of the GSK-J1 bioisostere KDOBA67 was determined against JMJD3, JARID1A, JARID1B, JARID1C, JMJD2C and JMJD1A (KDM families 3-6) using the ALPHAscreen (Amplified Luminescence Proximity Homogenous Assay) as previously described (9). This assay detects the product methyl mark using a methyl mark selective antibody coupled to a protein A acceptor bead and a streptavidin donor bead that captures a biotinylated peptide. Recombinant Jmj enzymes were produced in Ecoli or a baculovirus system (9,10). Enzyme reactions were stopped by addition of ethylenediaminetetraacetic acid (EDTA) and the presence of the biotinylated product methyl mark was detected using ALPHAscreen platform (Perkin Elmer). Inhibition assays were

performed in a 384-well plate format using white ProxiPlates (Perkin Elmer). Hydroxy ethyl piperazine ethane sulfonic acid (HEPES) buffer was from Life Technologies. Anti-Histone-H3-K9Me1 and anti-Histone-H3-K9Me2 antibodies were from Abcam, anti-Histone-H3-K27Me2 antibody was from Millipore, and anti-Histone-H3-K4Me2 antibody was from Cell Signaling Technology. Alphascreen General IgG detection kit was from Perkin Elmer. L-ascorbic acid (L-AA), ferrous ammonium sulphate (FAS), α-Ketoglutaric acid (α-KG) and bovine serum albumin (A7030) were from Sigma Aldrich. All in vitro assays were performed in assay buffer (50 mM HEPES pH7.5 containing 0.1% BSA and 0.01% Tween-20). Serial titrations of compounds (0.1 µl) were transferred into wells of a 384-well ProxiPlate using an Echo Acoustic dispenser (Labcyte) and Jmj enzyme (4.9 µl at 2X final assay concentration) was dispensed into each well and allowed to pre-incubate with compound for 15 minutes. Enzyme reactions were initiated by addition of 5 µl of a 2x substrate mix consisting of FAS, L-AA, α-KG and biotinylated peptide and the enzyme reaction progressed for the indicated times. The enzyme reaction was stopped by addition of 5 µl of assay buffer containing EDTA (7.5 mM final assay concentration) and NaCl (200 mM final assay concentration). Antibody to the product methyl mark was pre-incubated in the presence of Protein A acceptor beads (0.08 mg/ml) and Streptavidin donor beads (0.08 mg/ml) for 1 hour and the presence of biotin-H3-product in the assay was detected by addition of 5 µl of the pre-incubated alphascreen beads (final concentration of 0.02 mg/ml for acceptor and donor beads). After 1 hour incubation at room temperature the assay plates were read in a BMG Pherastar FS plate reader. Data were normalized to the no-enzyme control and the IC_{50} were determined from the nonlinear regression curve fit using GraphPad Prism 5.

Structure determination of UTY in complex with KDOBA67. A construct of human UTY (KDM6C) (encompassing aa residues Leu^{878}–Ser^{1347}) was expressed in Sf9 cells with a tobacco etch virus (TEV) protease-cleavable C-terminal His_{10}-tag, essentially as described (4). Generation of recombinant baculo virus, insect cell culture, and infections were performed according to the manufacturer's instructions (Invitrogen). The cells were suspended in a buffer containing 50 mM HEPES pH 7.5, 500 mM NaCl, 10 mM imidazole, 5% glycerol, 0.5 mM TCEP and a protease inhibitor mix (Calbiochem), and purified using nickel affinity chromatography with a stepwise gradient of imidazole after sonication. The eluted protein was then incubated with TEV protease at 4 °C overnight, followed by size exclusion chromatography (Superdex 200). The TEV protease and uncleaved protein were removed using nickel affinity chromatography, and the mass of the cleaved KDM6/UTY protein was verified by electrospray mass ionization time-of-flight mass spectrometry (Agilent LC/MSD).

Protein crystallisation, X-ray Data collection and structure determination. To crystallise UTY (KDM6C) with KDOBA67a, the protein (11 mg/mL) was preincubated with 1 mM of the inhibitor and 2 mM MnCl2. The protein-compound mixture was then transferred to crystallization plates using the sitting drop vapour diffusion method at 4 °C. Protein crystals were obtained in a drop consisting of 100 nL protein-compound and 100 nL of a precipitant consisting of 25% (w/v) PEG 3350, and 0.1 M bis-tris pH 6.5. Crystals were cryoprotected with mother liquor supplemented with 25% ethylene glycol before they were flash-frozen in liquid nitrogen. A data set with a diffraction limit of 2.0 Å was collected on beamline I04-1 at the Diamond Light source. The data were processed with XDS, scaled and merged using Aimless. The structure was determined by molecular replacement using UTY PDB ID 3ZLI (11) as a search model. The protein-ligand model was further improved by subsequent cycles of model building in coot and refinement in *REFMAC* (12). The refinement was terminated when there were no significant changes in the R_{work} and R_{free} values and inspection of the difference density maps suggested that no further corrections or additions were justified. The quality of the structure was assessed with the MolProbity server and deposited in Protein Data Bank with the PDB code 5A1L. Data collection and refinement statistics are given in **Table S3**.

Supplementary Acknowledgements

We would like to thank the Cancer Research UK Experimental Cancer Centre which provided support from the Genomics and Genome Engineering, Microscopy and Imaging, Pathology Services and Flow Cytometry Core facilities. AMF is a NIHR senior investigator, and the work was supported by the National Institute for Health Research, UCLH Biomedical Research Centre.

The Structural Genomics Consortium is a registered charity (number 1097737) that receives funds from Abbvie, Bayer Healthcare, Boehringer Ingelheim, the Canadian Institutes for Health Research, the Canadian Foundation for Innovation, Eli Lilly and Company, Genome Canada, GlaxoSmithKline, the Ontario Ministry of Economic Development and Innovation, Janssen, the Novartis Research Foundation, Pfizer, Takeda, and the Wellcome Trust.

Supplementary References

1. Ernst J, Kheradpour P, Mikkelsen TS, Shoresh N, Ward LD, Epstein CB, et al. Mapping and analysis of chromatin state dynamics in nine human cell types. Nature. Nature Publishing Group; 2011;473:43–9.
2. Miga KH, Eisenhart C, Kent WJ. Utilizing mapping targets of sequences underrepresented in the reference assembly to reduce false positive alignments. Nucleic Acids Res. 2015.
3. Thurman RE, Rynes E, Humbert R, Vierstra J, Maurano MT, Haugen E, et al. The accessible chromatin landscape of the human genome. Nature. 2012.
4. Bernstein BE, Birney E, Dunham I, Green ED, Gunter C, Snyder M. An integrated encyclopedia of DNA elements in the human genome. Nature [Internet]. 2012/09/08. 2012;489:57–74.
5. Sanjana NE, Shalem O, Zhang F. Improved vectors and genome-wide libraries for CRISPR screening. Nat Methods [Internet]. Nature Publishing Group; 2014;11:783–4.
6. Ohguchi H, Harada T, Sagawa M, Kikuchi S, Tai YT, Richardson PG, et al. KDM6B modulates MAPK pathway mediating multiple myeloma cell growth and survival. Leukemia [Internet]. Nature Publishing Group; 2017;31:2661–9.
7. Rohland N, Reich D. Cost-effective , high-throughput DNA sequencing. Genome Res. 2011;939–46.
8. Kruidenier L, Chung C, Cheng Z, Liddle J, Che K, Joberty G, et al. A selective jumonji H3K27 demethylase inhibitor modulates the proinflammatory macrophage response. Nature 2012;488:404–8.
9. Kawamura A, Tumber A, Rose NR, King ONF, Daniel M, Oppermann U, et al. Development of homogeneous luminescence assays for histone demethylase catalysis and binding. Anal Biochem. 2010;404:86–93.
10. Hatch SB, Yapp C, Montenegro RC, Savitsky P, Gamble V, Tumber A, et al. Assessing histone demethylase inhibitors in cells: Lessons learned. Epigenetics and Chromatin. 2017;10:1–17.
11. Walport LJ, Hopkinson RJ, Vollmar M, Madden SK, Gileadi C, Oppermann U, et al. Human UTY(KDM6C) is a Male-Specific Nϵ-Methyl Lysyl-Demethylase. J Biol Chem. 2014.
12. Lo WW, Pinnaduwage D, Gokgoz N, Wunder JS, Andrulis IL. Aberrant hedgehog signaling and clinical outcome in osteosarcoma. Sarcoma. 2014;2014:1–10.